



All-electrically tunable networks of Majorana bound states

Song-Bo Zhang ¹, Alessio Calzona ¹ and Björn Trauzettel^{1,2}¹*Institute for Theoretical Physics and Astrophysics, University of Würzburg, D-97074 Würzburg, Germany*²*Würzburg-Dresden Cluster of Excellence ct.qmat, Germany*

(Received 9 March 2020; accepted 28 August 2020; published 10 September 2020)

Second-order topological superconductors (SOTs) host localized Majorana fermions and provide a new platform for topological quantum computation. We propose a feasible way to realize networks based on SOTs which allow one to nucleate and braid Majorana bound states (MBSs) in an all-electrical manner without fine-tuning. The proposed setups are scalable in a straightforward way and can accommodate any even number of MBSs. Moreover, the MBSs in the networks allow defining qubits whose states can be initialized and read out by measuring Josephson currents flowing between SOT islands. Our proposal can be implemented in monolayers of FeTe_{1-x}Se_x, monolayers of 1T'-WTe₂, and inverted Hg(Cd)Te quantum wells in proximity to conventional superconductors.

DOI: [10.1103/PhysRevB.102.100503](https://doi.org/10.1103/PhysRevB.102.100503)

Introduction. Second-order topological superconductors (SOTs) are characterized by topologically protected midgap bound states with zero excitation energy and codimension two [1–12]. These midgap states behave like Majorana fermions which constitute their own antiparticles [13]. They obey non-Abelian exchange statistics and could find promising applications in topological quantum computation [14–20]. Recently, SOTs have been predicted in certain candidate systems [6–10, 21–37]. Hence, they provide a feasible platform for implementing topological quantum gates [38–40]. A few theoretical proposals have been made to explore the exchange of Majorana bound states (MBSs) in SOTs [40–43]. However, they are restricted to only a single pair of MBSs or require one to locally tune magnetic fields. To define a multidimensional computational ground-state manifold suitable for implementing non-Abelian quantum gates, four or more MBSs are required [16, 44]. Moreover, simpler manipulation schemes based on electrical controls are advantageous in experimental implementation and runtime for quantum gates.

In this Rapid Communication, we propose a way to realize electrically tunable networks of MBSs based on SOTs. We take full advantage of the special role played by the sample geometry in SOTs and conceive setups whose building blocks consist of isosceles right triangle islands (IRTIs) of SOTs. By modulating local gate voltages on the islands, it is possible to nucleate an arbitrary even number of MBSs and control their positions on the networks, allowing for non-Abelian braiding. The magnetic order in our proposal can be uniform. It can, for instance, be realized by in-plane ferromagnetism (FM), antiferromagnetism (AFM), Zeeman fields, or a mixture of them. Moreover, the qubit states defined by the MBSs in the network can be initialized and read out, for instance, by measuring Josephson currents flowing between the SOT islands. Importantly, our proposal can be implemented in a variety of candidate systems, including 1T'-WTe₂ monolayers, inverted Hg(Cd)Te quantum wells with proximity-induced

superconductivity, and FeTe_{1-x}Se_x monolayers with intrinsic superconductivity.

MBSs on open boundaries of SOTs. We consider two-dimensional SOTs which are realized by introducing *s*-wave pairing potential in combination with in-plane FM or AFM to quantum spin Hall insulators. The SOTs can be described by

$$\mathcal{H}(\mathbf{k}) = m(\mathbf{k})\tau_z\sigma_z + A \sin k_x s_z \sigma_x + A \sin k_y \tau_z \sigma_y - \mu\tau_z + \Delta_0\tau_y s_y + H_M \quad (1)$$

in the basis $(c_{a\uparrow}, c_{b\uparrow}, c_{a\downarrow}, c_{b\downarrow}, c_{a\uparrow}^\dagger, c_{b\uparrow}^\dagger, c_{a\downarrow}^\dagger, c_{b\downarrow}^\dagger)$, where $c_{\sigma s}$ is the fermion operator with orbital (or sublattice) index $\sigma \in \{a, b\}$ and spin index $s \in \{\uparrow, \downarrow\}$; $m(\mathbf{k}) = 2m \cos k_x + 2m \cos k_y + m_0 - 4m$ with $m_0 m > 0$; μ is the chemical potential controllable by external gates. The Pauli matrices \mathbf{s} , $\boldsymbol{\sigma}$, and $\boldsymbol{\tau}$ act on spin, orbital, and Nambu spaces, respectively. H_M describes the magnetic order. It can be induced by close proximity to ferromagnets or antiferromagnets or by applying in-plane magnetic fields. For concreteness, we focus on the case of FM with strength M_0 in the *x* direction, $H_M = M_0\tau_z s_x$ [45].

The SOTs feature zero-energy MBSs when open boundary conditions are enforced. To better understand this, it is instructive to derive a low-energy effective Hamiltonian on boundaries. We start with the low-energy limit of $\mathcal{H}(\mathbf{k})$ and consider the SOTs in a disk geometry of radius *R*. In the absence of M_0 and Δ_0 , we can find helical states $(\Psi_{e,\uparrow}, \Psi_{e,\downarrow}, \Psi_{h,\uparrow}, \Psi_{h,\downarrow})$ on the disk boundary. Using these helical states as a basis and projecting the full Hamiltonian $\mathcal{H}(\mathbf{k})$ on these states, the boundary Hamiltonian is constructed as

$$\tilde{\mathcal{H}}(\varphi) = -A p_\varphi s_z + \Delta_0 \tau_y s_y - \tilde{M} e^{-i\tau_z s_z \varphi} s_y - \mu \tau_z, \quad (2)$$

where φ is the azimuthal coordinate and $p_\varphi \equiv -i\partial_\varphi/R$ the corresponding momentum defined along the boundary. The boundary states possess effective pairing potential Δ_0 and magnetization $\tilde{M} = M_0 \sin \varphi$, as induced from the bulk. When

TABLE I. Fusion strength $F_{\gamma_i\gamma_j}$ of MBSs $\{\gamma_i\}$ and $\{\gamma_j\}$ belonging to two SOTS islands. The table displays the dependence of $F_{\gamma_i\gamma_j}$ on μ and μ' and on $\delta\Phi$. We define $\vartheta_{\pm} = (\vartheta \pm \vartheta')/2$, $\vartheta = \arctan(\mu/\Delta_0)$, and $\vartheta' = \arctan(\mu'/\Delta_0)$. Results for the fusion of MBSs belonging to the same island can be obtained by taking $\gamma'_i = \gamma_i$, $\delta\Phi = 0$, and $\mu' = \mu$.

	γ_1	γ_2	γ_3	γ_4
γ'_1	$\sin \vartheta_- \sin \delta\Phi$	$\cos \vartheta_+ \cos \delta\Phi$	$\cos \vartheta_- \sin \delta\Phi$	$\sin \vartheta_+ \cos \delta\Phi$
γ'_2	$\cos \vartheta_+ \cos \delta\Phi$	$\sin \vartheta_- \sin \delta\Phi$	$\sin \vartheta_+ \cos \delta\Phi$	$\cos \vartheta_- \sin \delta\Phi$
γ'_3	$\cos \vartheta_- \sin \delta\Phi$	$\sin \vartheta_+ \cos \delta\Phi$	$\sin \vartheta_- \sin \delta\Phi$	$\cos \vartheta_+ \cos \delta\Phi$
γ'_4	$\sin \vartheta_+ \cos \delta\Phi$	$\cos \vartheta_- \sin \delta\Phi$	$\cos \vartheta_+ \cos \delta\Phi$	$\sin \vartheta_- \sin \delta\Phi$

$M_0 > \bar{\Delta} \equiv (\Delta_0^2 + \mu^2)^{1/2}$, we find that the energy bands of Eq. (2) change their order at the angles

$$\varphi_{1/4} = \pm \arcsin(\bar{\Delta}/M_0) \quad \text{and} \quad \varphi_{2/3} = \varphi_{4/1} + \pi \quad (3)$$

along the boundary. The changes of band order indicate the appearance of four MBSs γ_i with $i \in \{1, 2, 3, 4\}$, exponentially localized at φ_i . When they are well separated from each other, the four MBSs are at zero energy and it is possible to analytically derive their wave functions Ψ_i [46]. Importantly, the chemical potential μ controls the angles φ_i , according to Eq. (3). This enables us to manipulate the positions of the MBSs, and eventually their fusion and braiding in an all-electrical manner, as discussed below.

Fusion properties of MBSs. When two MBSs are brought close together, their wave functions start to overlap and their energies become finite. This process, known as fusion, is mediated by the electron hopping in the SOTSs. According to Eq. (1), the hopping corresponds to the operator $\hat{T} = iA(s_z\sigma_x + \tau_z\sigma_y)/2 + 2m\tau_z\sigma_z$. Thus, the fusion strength between two MBSs, say γ_i and γ_j , can be estimated as $F_{\gamma_i\gamma_j} = |\langle \Psi_i | \hat{T} | \Psi_j \rangle|$. On a single island, we find that the fusion strengths $F_{\gamma_1\gamma_2}$ and $F_{\gamma_3\gamma_4}$ are proportional to $\cos \vartheta$, while $F_{\gamma_1\gamma_4}$ and $F_{\gamma_2\gamma_3}$ to $\sin \vartheta$, where $\vartheta = \arctan(\mu/\Delta_0)$. By contrast, the fusion between γ_1 and γ_3 (or γ_2 and γ_4) is strictly forbidden, due to inversion symmetry of the SOTSs [46].

The fusion properties become richer when we consider two sets of MBSs $\{\gamma_i\}$ and $\{\gamma'_i\}$ (with $i \in \{1, 2, 3, 4\}$) belonging to two different islands, featuring a finite pairing phase difference. In this case, when two MBSs from different islands are brought close together, they can always fuse in general. The mutual fusion strengths $F_{\gamma_i\gamma'_j}$ are summarized in Table I and depend sinusoidally on the pairing phase difference $2\delta\Phi$ and the chemical potentials μ and μ' of the two islands.

Manipulation of MBSs in IRTIs. In order to obtain a scalable platform hosting any even number of MBSs which are manipulable by purely electrical means, it is essential to go beyond the simple disk geometry presented so far. Particularly, we focus on IRTIs, the short sides of which are orientated in the x and y directions, as depicted in Fig. 1. To develop some intuition about the appearance of MBSs in the IRTIs, one can relate the latter to the disk geometry in the following way: the dotted lines normal to the triangle sides define three arcs of the disk boundary (dashed curves); all the points belonging to the same arc reduce to the corresponding vertex of the triangle (colored arrows); conversely, each side of the triangle reduces

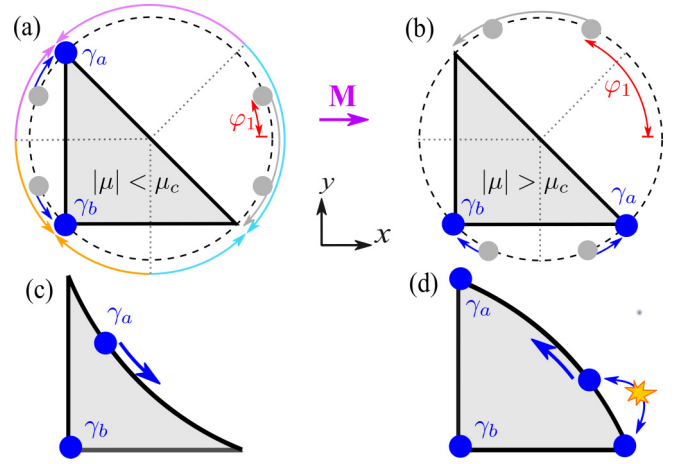


FIG. 1. Positions of two MBSs (blue dots) in an IRTI for (a) $|\mu| < \mu_c$ and (b) $|\mu| > \mu_c$, respectively. The gray dots denote the four MBSs on a disk boundary (dashed curve). The magnetic order (M) is fixed in the x direction. By increasing μ from $0 < \mu < \mu_c$ to $\mu > \mu_c$, the angle φ_1 (in red) increases and one MBS is moved from one sharp-angle vertex to the other one. Schematics of IRTIs with small concavity (c) or convexity (d) on the diagonals.

to a single point on the disk. Out of the four MBSs (gray dots) hosted by the disk, two of them must locate on the same arc meaning that, in the triangle, they fuse on the same vertex. By contrast, the two remaining MBSs locate on different arcs and thus stay robustly as zero-energy corner states (blue dots) in the IRTI. Which vertices host the MBSs crucially depends on the angles φ_i (φ_1 is depicted in red) and, therefore, on the value of the chemical potential μ .

For $|\mu| < \mu_c \equiv (M_0^2/2 - \Delta_0^2)^{1/2}$, the four MBSs on the disk are sketched in Fig. 1(a). For $|\mu| > \mu_c$, the MBSs are located as shown in Fig. 1(b). By slowly tuning μ across μ_c , say from $\mu_d (< \mu_c)$ to $\mu_u (> \mu_c)$, we can thus adiabatically move one MBS between two sharp-angle vortices while the other one stays fixed at the right-angle vertex. We observe that a finite μ_c requires $M_0 > \sqrt{2}\Delta_0$. When μ is close to μ_c , the localization length of the movable MBS along the diagonal is approximately proportional to $A\Delta_0/(\mu_c|\mu - \mu_c|)$. Therefore, larger islands pose weaker constraints on the difference $\mu_u - \mu_d$. The possibility to move MBSs between two vertices is confirmed numerically [46]. These results apply to any IRTIs with the short sides in the x and y directions.

To get more insight into the fundamental role played by the SOTS geometry and to make further use of it, we consider a small bending on the diagonal. Interestingly, we find that small concavity on the diagonal allows us to smoothly move the MBS along the diagonal [Fig. 1(c)]. It also helps to enhance the excitation gap that protects the MBSs since the diagonal becomes fully gapped everywhere except for one point in space even at μ_c [46]. By contrast, small convexity tends to nucleate an extra Majorana pair and thus momentarily increases the ground-state degeneracy [Fig. 1(d)].

Building networks of MBSs. By properly connecting several IRTIs, networks of diagonals can be defined, for instance, as sketched in Fig. 2 (more examples are given in the Supplemental Material [46]). When two or more vertices get in contact, there is a finite overlap between the wave functions

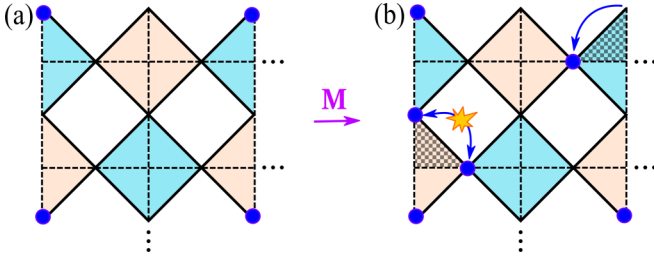


FIG. 2. Networks of connected IRTIs. The cyan and yellow colors distinguish between two pairing phases on the islands. The white regions are vacuum or trivial insulator. The dashed lines mark the boundaries between the IRTIs. In (a), all $\mu_j = \mu_d$ and the network hosts four MBSs indicated by the blue dots. In (b), the chemical potentials of triangles marked by the shadow pattern have been tuned to μ_u , resulting in the movement of the top-right MBS and in the nucleation of two additional MBSs.

of different MBSs, which fuse according to the inter- and intraisland fusion strengths summarized in Table I. The latter clearly depends on the chemical potential and the superconducting phases Φ_j of adjacent IRTIs. For concreteness, in the following, we focus on the configuration illustrated in Fig. 2, where we apply $\Phi_j = 0$ for the cyan triangles and $\Phi_j = \Phi_0 \neq p\pi$ (with $p \in \mathbb{Z}$) for the yellow ones. As a result, we observe that every time an even number of MBSs approach the same point, they completely fuse. Conversely, when an odd number of MBSs approach the same point, a single MBS is left at zero energy.

By tuning the chemical potentials of individual IRTIs across μ_c , it is therefore possible to either nucleate, fuse, or move MBSs on the network. Two clarifying examples are illustrated in Fig. 2. In Fig. 2(a), all chemical potentials are set to $\mu_d < \mu_c$, resulting in the presence of four MBSs. In Fig. 2(b), the chemical potentials of two IRTIs (highlighted by a shadow pattern) have been tuned to $\mu_u > \mu_c$. Consequently, the top-right MBS is moved while a new pair of MBSs has been nucleated in the left-bottom of the network.

It is important to stress that the Majorana manipulation does not rely on fine-tuning of parameters. The proposed setup can therefore be easily scaled up, just by adding more IRTIs, in order to accommodate an arbitrary number of MBSs. Since each MBS is exponentially localized on a specific node of the network, the lifting of the ground-state degeneracy is exponentially small in the size of each island.

Braiding a Majorana qubit. To illustrate the capabilities of our networks, we now show how to braid a couple of MBSs, thus implementing a phase gate on a Majorana qubit. The latter consists of four MBSs, which can be hosted by the six-island structure depicted in Fig. 3. We label the IRTIs by T_j (with $j \in \{1, \dots, 6\}$) and the corresponding chemical potentials and superconducting phases by μ_j and Φ_j , respectively. For the numerical simulation illustrated in Fig. 3, we considered $\Phi_5 = \Phi_6 = \pi/2$ and $\Phi_j = 0$ otherwise.

The initial configuration, Fig. 3(a), features $\mu_j = \mu_u$ for $j \in \{1, 5, 6\}$ and $\mu_j = \mu_d$ otherwise. We can observe four MBSs which are indicated by the black localized densities and labeled by $\gamma_a, \gamma_b, \gamma_c$, and γ_d . In order to braid γ_a and γ_b , the chemical potentials μ_4, μ_5 , and μ_6 must be adiabatically

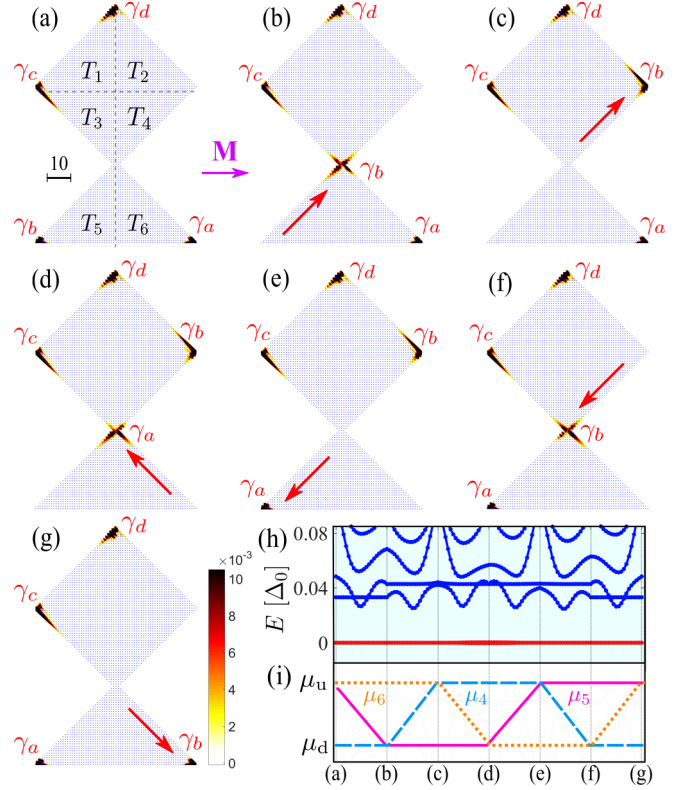


FIG. 3. Numerical simulation of braiding γ_a and γ_b . (a)–(g) Seven subsequent snapshots show the positions of the four MBSs (black localized densities). During the protocol, μ_4, μ_5 , and μ_6 are varied in time, according to (i), while $\mu_1 = \mu_u$ and $\mu_2 = \mu_3 = \mu_d$ are fixed. (h) The energy spectrum of the system during the process. It is symmetric with respect to zero energy. The parameters are $\mu_u = 0.15m_0$, $\mu_d = 0.05m_0$, $M_0 = 0.4m_0$, $\Delta_0 = 0.25m_0$, and $A = m = 0.5m_0$; the short-side length of the IRTIs is $L = 35a$.

tuned in time, according to Fig. 3(i). This results in the motion of γ_a and γ_b along the diagonals of T_4, T_5 , and T_6 , as shown in Figs. 3(a)–3(g). At the end of the protocol, while the system has the same parameters as in the initial state, the positions of γ_a and γ_b are exchanged. Importantly, during the whole process, the four MBSs stay robustly at zero energy [red bands in Fig. 3(h)]. They are always separated from excited states (blue bands) by an energy gap. Similar procedures apply to exchange other MBS pairs [46].

Because of the non-Abelian nature of MBSs, the braiding of γ_a and γ_b results in a nontrivial unitary operation $U_{ab} = \exp(\pi\gamma_a\gamma_b/4)$ on the Majorana qubit [14]. It corresponds to a quantum gate that implements a $\pi/2$ rotation on the Bloch sphere. This can be experimentally confirmed by measuring the parity of two different couples of MBSs, $P_{bc} = i\gamma_b\gamma_c$ and $P_{ac} = i\gamma_a\gamma_c$. The former one can be used to initialize the qubit, say in the eigenstate of $P_{bc}|0\rangle = |0\rangle$. Then, the braiding rotates the initial state to $U_{ab}|0\rangle$ which is an eigenstate of $P_{ac}U_{ab}|0\rangle = U_{ab}|0\rangle$. The validity of this result can be straightforwardly verified by measuring P_{ac} .

Remarkably, our all-in-one setup allows for initialization, braiding, and readout. Indeed, because of the possibility to move and fuse arbitrary couples of MBSs on the network, we can measure a generic parity operator $P_{\alpha\beta}$. For concreteness,

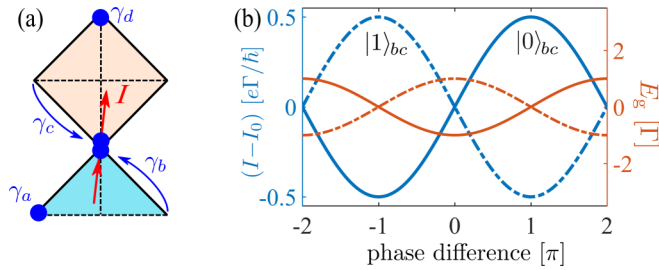


FIG. 4. (a) Detection of the parity P_{bc} of γ_b and γ_c by measuring the Josephson current. (b) Ground-state energy E_g (orange curves) of the two coupled MBSs, γ_b and γ_c , and the Josephson current (blue curves) across the junction as functions of the pairing phase difference. Solid and broken curves correspond to the two parity states, $P_{bc}|0\rangle_{bc} = |0\rangle_{bc}$ and $P_{bc}|1\rangle_{bc} = -|1\rangle_{bc}$.

we describe the measurement of P_{bc} in the six-island architecture. In this case, one must fuse γ_b and γ_c by moving them in the region which defines a Josephson junction between islands with different pairing phases [Fig. 4(a)]. The effective Hamiltonian which describes the coupling between the two MBSs reads $\mathcal{H}_{bc} = \Gamma \cos(\delta\Phi)P_{bc}$, where $2\delta\Phi$ is the pairing phase difference and Γ is the coupling strength that depends on the chemical potentials and wave-function overlap. The two eigenenergies are therefore $E_g = \pm\Gamma \cos(\delta\Phi)$ [orange curves in Fig. 4(b)]. At zero temperature, the Josephson current across the junction is $I = I_0 \mp e\Gamma \sin(\delta\Phi)/2\hbar = I_0 \mp I_{\text{mbs}}$, where I_{mbs} and I_0 are the contributions from the MBSs and ordinary fermions, respectively [47]. As long as $2\delta\Phi \neq 0$, by probing I flowing between the islands one can therefore measure P_{bc} [Fig. 4(b)]. In principle, other measurement schemes based on quantum dots are also possible [46,49].

Experimental feasibility and summary. Remarkably, $\text{FeTe}_{1-x}\text{Se}_x$ monolayers have been shown to possess a band inversion at the Γ point [50–52] and intrinsic high-temperature superconductivity [53]. The magnetic order may be induced by putting (anti)ferromagnets, e.g., FeSe or FeTe layers [54–56], on top of $\text{FeTe}_{1-x}\text{Se}_x$ monolayers or by applying in-plane magnetic fields. We note that the sustenance of superconductivity under strong in-plane magnetic fields in this material has been reported experimentally [57]. Interestingly, FeSe monolayers coupling to substrates may have all the desired ingredients for realizing SOTs (namely, band inversions at the M points, superconductivity [58–60], and AFM

order [61]) intrinsically within one material. Quantum spin Hall insulators, such as monolayers of $1T'$ - WTe_2 [62–68], inverted Hg(Cd)Te, and InAs/GaSb quantum wells [69–75], in proximity to conventional superconductors could offer another candidate system. Notably, electric gating on superconducting $1T'$ - WTe_2 monolayers has already been demonstrated [66,67].

In general, the control of local chemical potentials on the islands might be a challenging task. However, it is by no means necessary to fine-tune the chemical potentials to specific values of μ_u and μ_d . The only requirements are (i) the possibility to tune μ across its critical value, i.e., $\mu_d < \mu_c < \mu_u$, and (ii) that, at μ_u and μ_d , the MBSs are well localized at the vertices of IRTIs. Importantly, we numerically prove that inhomogeneities of chemical potential within each IRTI are not detrimental to our proposal [46]. Finally, we remark that field effects on (superconducting) thin films have proven to be a valid alternative to conventional chemical doping in order to tune the carrier density [76–78], suggesting the feasibility of controlling local chemical potentials with external gates.

An important issue, when it comes to Majorana-based quantum computation, is represented by quasiparticle poisoning (QP) [79–81], causing detrimental flips in the total fermion parity of individual qubits. In this respect, the large superconducting gap of $\text{FeTe}_{1-x}\text{Se}_x$ monolayers (up to 16.5 meV [53]) represents a prime advantage: (i) It is likely to decrease the QP rate. (ii) It allows for faster adiabatic qubit operations. Moreover, it might be possible to implement quasiparticle filters which have proven, at least for quantum wires, to increase the characteristic QP time up to (1/200) s [82].

In summary, we have proposed a feasible way to realize networks of SOTs which can accommodate any even number of topologically protected MBSs. The MBSs can be generated, moved, and fused by all-electrical means. Our proposal allows one to define a qubit, braid the corresponding MBSs, and measure the nontrivial outcome of this operation.

Acknowledgments. We thank Sang-Jun Choi, Ning Hao, Tobias Kiessling, and Wenbin Rui for valuable discussion. This work was supported by the DFG (SPP1666 and SFB1170 “ToCoTronics”), the Würzburg-Dresden Cluster of Excellence ct.qmat, EXC2147, Project ID No. 390858490, and the Elitenetzwerk Bayern Graduate School on “Topological Insulators.”

S.-B.Z. and A.C. contributed equally to this work.

- [1] J. Langbehn, Y. Peng, L. Trifunovic, F. von Oppen, and P. W. Brouwer, Reflection-Symmetric Second-Order Topological Insulators and Superconductors, *Phys. Rev. Lett.* **119**, 246401 (2017).
- [2] W. A. Benalcazar, B. A. Bernevig, and T. L. Hughes, Quantized electric multipole insulators, *Science* **357**, 61 (2017).
- [3] Z. Song, Z. Fang, and C. Fang, $(d-2)$ -Dimensional Edge States of Rotation Symmetry Protected Topological States, *Phys. Rev. Lett.* **119**, 246402 (2017).

- [4] W. A. Benalcazar, B. A. Bernevig, and T. L. Hughes, Electric multipole moments, topological multipole moment pumping, and chiral hinge states in crystalline insulators, *Phys. Rev. B* **96**, 245115 (2017).
- [5] F. Schindler, A. M. Cook, M. G. Vergniory, Z. Wang, S. S. P. Parkin, B. A. Bernevig, and T. Neupert, Higher-order topological insulators, *Sci. Adv.* **4**, eaat0346 (2018).
- [6] Q. Wang, C.-C. Liu, Y.-M. Lu, and F. Zhang, High-Temperature Majorana Corner States, *Phys. Rev. Lett.* **121**, 186801 (2018).

- [7] Z. Yan, F. Song, and Z. Wang, Majorana Corner Modes in a High-Temperature Platform, *Phys. Rev. Lett.* **121**, 096803 (2018).
- [8] T. Liu, J. J. He, and F. Nori, Majorana corner states in a two-dimensional magnetic topological insulator on a high-temperature superconductor, *Phys. Rev. B* **98**, 245413 (2018).
- [9] M. Geier, L. Trifunovic, M. Hoskam, and P. W. Brouwer, Second-order topological insulators and superconductors with an order-two crystalline symmetry, *Phys. Rev. B* **97**, 205135 (2018).
- [10] H. Shapourian, Y. Wang, and S. Ryu, Topological crystalline superconductivity and second-order topological superconductivity in nodal-loop materials, *Phys. Rev. B* **97**, 094508 (2018).
- [11] A. Skurativska, T. Neupert, and M. H. Fischer, Atomic limit and inversion-symmetry indicators for topological superconductors, *Phys. Rev. Res.* **2**, 013064 (2020).
- [12] A. Tiwari, M.-H. Li, B. A. Bernevig, T. Neupert, and S. A. Parameswaran, Unhinging the Surfaces of Higher-Order Topological Insulators and Superconductors, *Phys. Rev. Lett.* **124**, 046801 (2020).
- [13] E. Majorana, Teoria simmetrica dell'elettrone e del positrone, *Nuovo Cimento* **14**, 171 (1937).
- [14] D. A. Ivanov, Non-Abelian Statistics of Half-Quantum Vortices in p -Wave Superconductors, *Phys. Rev. Lett.* **86**, 268 (2001).
- [15] A. Y. Kitaev, Fault-tolerant quantum computation by anyons, *Ann. Phys.* **303**, 2 (2003).
- [16] C. Nayak, S. H. Simon, A. Stern, M. Freedman, and S. Das Sarma, Non-Abelian anyons and topological quantum computation, *Rev. Mod. Phys.* **80**, 1083 (2008).
- [17] J. Alicea, New directions in the pursuit of Majorana fermions in solid state systems, *Rep. Prog. Phys.* **75**, 076501 (2012).
- [18] C. W. J. Beenakker, Search for Majorana fermions in superconductors, *Annu. Rev. Condens. Matter Phys.* **4**, 113 (2013).
- [19] S. Das Sarma, M. Freedman, and C. Nayak, Majorana zero modes and topological quantum computation, *npj Quantum Inf.* **1**, 15001 (2015).
- [20] S. R. Elliott and M. Franz, Colloquium: Majorana fermions in nuclear, particle, and solid-state physics, *Rev. Mod. Phys.* **87**, 137 (2015).
- [21] C.-H. Hsu, P. Stano, J. Klinovaja, and D. Loss, Majorana Kramers Pairs in Higher-Order Topological Insulators, *Phys. Rev. Lett.* **121**, 196801 (2018).
- [22] Y. Volpez, D. Loss, and J. Klinovaja, Second-Order Topological Superconductivity in π -Junction Rashba Layers, *Phys. Rev. Lett.* **122**, 126402 (2019).
- [23] S.-B. Zhang and B. Trauzettel, Detection of second-order topological superconductors by Josephson junctions, *Phys. Rev. Res.* **2**, 012018 (2020).
- [24] S. A. A. Ghorashi, X. Hu, T. L. Hughes, and E. Rossi, Second-order Dirac superconductors and magnetic field induced Majorana hinge modes, *Phys. Rev. B* **100**, 020509(R) (2019).
- [25] R.-X. Zhang, W. S. Cole, X. Wu, and S. Das Sarma, Higher-Order Topology and Nodal Topological Superconductivity in Fe(Se,Te) Heterostructures, *Phys. Rev. Lett.* **123**, 167001 (2019).
- [26] K. Plekhanov, M. Thakurathi, D. Loss, and J. Klinovaja, Floquet second-order topological superconductor driven via ferromagnetic resonance, *Phys. Rev. Res.* **1**, 032013 (2019).
- [27] J. Ahn and B.-J. Yang, Higher-order topological duperconductivity of dpin-polarized fermions, *Phys. Rev. Res.* **2**, 012060 (2020).
- [28] S. Franca, D. V. Efremov, and I. C. Fulga, Phase-tunable second-order topological superconductor, *Phys. Rev. B* **100**, 075415 (2019).
- [29] R.-X. Zhang, W. S. Cole, and S. Das Sarma, Helical Hinge Majorana Modes in Iron-Based Superconductors, *Phys. Rev. Lett.* **122**, 187001 (2019).
- [30] N. Bultinck, B. A. Bernevig, and M. P. Zaletel, Three-dimensional superconductors with hybrid higher-order topology, *Phys. Rev. B* **99**, 125149 (2019).
- [31] Y.-T. Hsu, W. S. Cole, R.-X. Zhang, and J. D. Sau, Inversion-Protected Higher-Order Topological Superconductivity in Monolayer WTe₂, *Phys. Rev. Lett.* **125**, 097001 (2020).
- [32] Z. Yan, Higher-Order Topological Odd-Parity Superconductors, *Phys. Rev. Lett.* **123**, 177001 (2019).
- [33] X.-H. Pan, K.-J. Yang, L. Chen, G. Xu, C.-X. Liu, and X. Liu, Lattice-Symmetry-Assisted Second-Order Topological Superconductors and Majorana Patterns, *Phys. Rev. Lett.* **123**, 156801 (2019).
- [34] Y. Peng, Floquet higher-order topological insulators and superconductors with space-time symmetries, *Phys. Rev. Res.* **2**, 013124 (2020).
- [35] Y.-J. Wu, J. Hou, Y.-M. Li, X.-W. Luo, X. Shi, and C. Zhang, In-Plane Zeeman-Field-Induced Majorana Corner and Hinge Modes in an s -Wave Superconductor Heterostructure, *Phys. Rev. Lett.* **124**, 227001 (2020).
- [36] K. Laubscher, D. Loss, and J. Klinovaja, Majorana and parafermion corner states from two coupled sheets of bilayer graphene, *Phys. Rev. Res.* **2**, 013330 (2020).
- [37] X. Wu, X. Liu, R. Thomale, and C.-X. Liu, High- T_c superconductor Fe(Se,Te) monolayer: An intrinsic, scalable and electrically-tunable Majorana platform, [arXiv:1905.10648](https://arxiv.org/abs/1905.10648).
- [38] Y. You, D. Litinski, and F. von Oppen, Higher-order topological superconductors as generators of quantum codes, *Phys. Rev. B* **100**, 054513 (2019).
- [39] R. W. Bomantara and J. Gong, Measurement-only quantum computation with Floquet Majorana corner modes, *Phys. Rev. B* **101**, 085401 (2020).
- [40] S.-B. Zhang, W. B. Rui, A. Calzona, S.-J. Choi, A. P. Schnyder, and B. Trauzettel, Topological and holonomic quantum computation based on second-order topological superconductors, [arXiv:2002.05741](https://arxiv.org/abs/2002.05741).
- [41] X. Zhu, Tunable Majorana corner states in a two-dimensional second-order topological superconductor induced by magnetic fields, *Phys. Rev. B* **97**, 205134 (2018).
- [42] M. Ezawa, Braiding of Majorana-like corner states in electric circuits and its non-Hermitian generalization, *Phys. Rev. B* **100**, 045407 (2019).
- [43] T. E. Pahomi, M. Sigrist, and A. A. Soluyanov, Braiding Majorana corner modes in a two-layer second-order topological insulator, [arXiv:1904.07822](https://arxiv.org/abs/1904.07822).
- [44] S. Bravyi, Universal quantum computation with the $\nu = 5/2$ fractional quantum Hall state, *Phys. Rev. A* **73**, 042313 (2006).
- [45] We note, however, that our main results discussed below also apply to other cases; for instance, AFM with $H_M = M_0 \tau_z \sigma_x$.
- [46] See Supplemental Material at <http://link.aps.org/supplemental/10.1103/PhysRevB.102.100503> for details, and which includes Refs. [48–50,69].

- [47] L. Fu and C. L. Kane, Superconducting Proximity Effect and Majorana Fermions at the Surface of a Topological Insulator, *Phys. Rev. Lett.* **100**, 096407 (2008).
- [48] J. Alicea, Y. Oreg, G. Refael, F. Von Oppen, and M. P. A. Fisher, Non-Abelian statistics and topological quantum information processing in 1D wire networks, *Nat. Phys.* **7**, 412 (2011).
- [49] K. Flensberg, Non-Abelian Operations on Majorana Fermions via Single-Charge Control, *Phys. Rev. Lett.* **106**, 090503 (2011).
- [50] X. Wu, S. Qin, Y. Liang, H. Fan, and J. Hu, Topological characters in $\text{Fe}(\text{Te}_{1-x}\text{Se}_x)$ thin films, *Phys. Rev. B* **93**, 115129 (2016).
- [51] X. Shi, Z.-Q. Han, P. Richard, X.-X. Wu, X.-L. Peng, T. Qian, S.-C. Wang, J.-P. Hu, Y.J. Sun, and H. Ding, $\text{FeTe}_{1-x}\text{Se}_x$ monolayer films: Towards the realization of high-temperature connate topological superconductivity, *Sci. Bull.* **62**, 503 (2017).
- [52] X.-L. Peng, Y. Li, X.-X. Wu, H.-B. Deng, X. Shi, W.-H. Fan, M. Li, Y.-B. Huang, T. Qian, P. Richard, J.-P. Hu, S.-H. Pan, H.-Q. Mao, Y.-J. Sun, and H. Ding, Observation of topological transition in high- T_c superconducting monolayer $\text{FeTe}_{1-x}\text{Se}_x$ films on $\text{SrTiO}_3(001)$, *Phys. Rev. B* **100**, 155134 (2019).
- [53] F. Li, H. Ding, C. Tang, J. Peng, Q. Zhang, W. Zhang, G. Zhou, D. Zhang, C.-L. Song, K. He, S. Ji, X. Chen, L. Gu, L. Wang, X.-C. Ma, and Q.-K. Xue, Interface-enhanced high-temperature superconductivity in single-unit-cell $\text{FeTe}_{1-x}\text{Se}_x$ films on SrTiO_3 , *Phys. Rev. B* **91**, 220503(R) (2015).
- [54] F. Ma, W. Ji, J. Hu, Z.-Y. Lu, and T. Xiang, First-Principles Calculations of the Electronic Structure of Tetragonal α -FeTe and α -FeSe Crystals: Evidence for a Bicollinear Antiferromagnetic Order, *Phys. Rev. Lett.* **102**, 177003 (2009).
- [55] W. Bao, Y. Qiu, Q. Huang, M. A. Green, P. Zajdel, M. R. Fitzsimmons, M. Zhernenkov, S. Chang, M. Fang, B. Qian, E. K. Vehstedt, J. Yang, H. M. Pham, L. Spinu, and Z. Q. Mao, Tunable $(\delta\pi, \delta\pi)$ -Type Antiferromagnetic Order in α -Fe(Te,Se) Superconductors, *Phys. Rev. Lett.* **102**, 247001 (2009).
- [56] S. Manna, A. Kamlapure, L. Cornils, T. Hänke, E. M. J. Hedegaard, M. Bremholm, B. B. Iversen, P. Hofmann, J. Wiebe, and R. Wiesendanger, Interfacial superconductivity in a bicollinear antiferromagnetically ordered FeTe monolayer on a topological insulator, *Nat. Commun.* **8**, 14074 (2017).
- [57] M. B. Salamon, N. Cornell, M. Jaime, F. F. Balakirev, A. Zakhidov, J. Huang, and H. Wang, Upper Critical Field and Kondo Effects in $\text{Fe}(\text{Te}_{0.9}\text{Se}_{0.1})$ Thin Films by Pulsed Field Measurements, *Sci. Rep.* **6**, 21469 (2016).
- [58] N. Hao and J. Hu, Topological Phases in the Single-Layer FeSe, *Phys. Rev. X* **4**, 031053 (2014).
- [59] N. Hao and J. Hu, Topological quantum states of matter in iron-based superconductors: From concept to material realization, *Nat. Sci. Rev.* **6**, 213 (2018).
- [60] Z. F. Wang, H. Zhang, D. Liu, C. Liu, C. Tang, C. Song, Y. Zhong, J. Peng, F. Li, C. Nie *et al.*, Topological edge states in a high-temperature superconductor $\text{FeSe}/\text{SrTiO}_3(001)$ film, *Nat. Mater.* **15**, 968 (2016).
- [61] S. He, J. He, W. Zhang, L. Zhao, D. Liu, X. Liu, D. Mou, Y.-B. Ou, Q.-Y. Wang, Z. Li *et al.*, Phase diagram and electronic indication of high-temperature superconductivity at 65 K in single-layer FeSe films, *Nat. Mater.* **12**, 605 (2013).
- [62] X. Qian, J. Liu, L. Fu, and J. Li, Quantum spin Hall effect in two-dimensional transition metal dichalcogenides, *Science* **346**, 1344 (2014).
- [63] S. Wu, V. Fatemi, Q. D. Gibson, K. Watanabe, T. Taniguchi, R. J. Cava, and P. Jarillo-Herrero, Observation of the quantum spin Hall effect up to 100 kelvin in a monolayer crystal, *Science* **359**, 76 (2018).
- [64] Z. Fei, T. Palomaki, S. Wu, W. Zhao, X. Cai, B. Sun, P. Nguyen, J. Finney, X. Xu, and D. H. Cobden, Edge conduction in monolayer WTe_2 , *Nat. Phys.* **13**, 677 (2017).
- [65] S. Tang, C. Zhang, D. Wong, Z. Pedramrazi, H.-Z. Tsai, C. Jia, B. Moritz, M. Claassen, H. Ryu, S. Kahn *et al.*, Quantum spin Hall state in monolayer $1T'$ - WTe_2 , *Nat. Phys.* **13**, 683 (2017).
- [66] E. Sajadi, T. Palomaki, Z. Fei, W. Zhao, P. Bement, C. Olsen, S. Luescher, X. Xu, J. A. Folk, and D. H. Cobden, Gate-induced superconductivity in a monolayer topological insulator, *Science* **362**, 922 (2018).
- [67] V. Fatemi, S. Wu, Y. Cao, L. Bretheau, Q. D. Gibson, K. Watanabe, T. Taniguchi, R. J. Cava, and P. Jarillo-Herrero, Electrically tunable low-density superconductivity in a monolayer topological insulator, *Science* **362**, 926 (2018).
- [68] F. Lüpke, D. Waters, C. Sergio, M. Widom, D. G. Mandrus, J. Yan, R. M. Feenstra, and B. M. Hunt, Proximity-induced superconducting gap in the quantum spin Hall edge state of monolayer WTe_2 , *Nat. Phys.* **16**, 526 (2020).
- [69] B. A. Bernevig, T. L. Hughes, and S.-C. Zhang, Quantum Spin Hall Effect and Topological Phase Transition in HgTe Quantum Wells, *Science* **314**, 1757 (2006).
- [70] M. König, S. Wiedmann, C. Brüne, A. Roth, H. Buhmann, L. W. Molenkamp, X.-L. Qi, and S.-C. Zhang, Quantum spin Hall insulator state in HgTe quantum wells, *Science* **318**, 766 (2007).
- [71] C. Liu, T. L. Hughes, X.-L. Qi, K. Wang, and S.-C. Zhang, Quantum Spin Hall Effect in Inverted Type-II Semiconductors, *Phys. Rev. Lett.* **100**, 236601 (2008).
- [72] I. Knez, R. R. Du, and G. Sullivan, Evidence for Helical Edge Modes in Inverted InAs/GaSb Quantum Wells, *Phys. Rev. Lett.* **107**, 136603 (2011).
- [73] S. Hart, H. Ren, T. Wagner, P. Leubner, M. Mühlbauer, C. Brüne, H. Buhmann, L. W. Molenkamp, and A. Yacoby, Induced superconductivity in the quantum spin Hall edge, *Nat. Phys.* **10**, 638 (2014).
- [74] S. Hart, H. Ren, M. Kosowsky, G. Ben-Shach, P. Leubner, C. Brüne, H. Buhmann, L. W. Molenkamp, B. I. Halperin, and A. Yacoby, Controlled finite momentum pairing and spatially varying order parameter in proximitized HgTe quantum wells, *Nat. Phys.* **13**, 87 (2017).
- [75] H. Ren, F. Pientka, S. Hart, A. T. Pierce, M. Kosowsky, L. Lunczer, R. Schlereth, B. Scharf, E. M. Hankiewicz, L. W. Molenkamp *et al.*, Topological superconductivity in a phase-controlled Josephson junction, *Nature (London)* **569**, 93 (2019).
- [76] A.M. Goldman, Electrostatic gating of ultrathin films, *Annu. Rev. Mater. Res.* **44**, 45 (2014).
- [77] K. Hanzawa, H. Sato, H. Hiramatsu, T. Kamiya, and H. Hosono, Electric field-induced superconducting transition of insulating FeSe thin film at 35 K, *Proc. Natl. Acad. Sci. U.S.A.* **113**, 3986 (2016).
- [78] J. Hänisch, K. Iida, R. Hüne, and C. Tarantini, Fe-based superconducting thin films—Preparation and tuning of superconducting properties, *Supercond. Sci. Technol.* **32**, 093001 (2019).

- [79] G. Goldstein and C. Chamon, Decay rates for topological memories encoded with Majorana fermions, *Phys. Rev. B* **84**, 205109 (2011).
- [80] J. C. Budich, S. Walter, and B. Trauzettel, Failure of protection of Majorana based qubits against decoherence, *Phys. Rev. B* **85**, 121405(R) (2012).
- [81] D. Rainis and D. Loss, Majorana qubit decoherence by quasiparticle poisoning, *Phys. Rev. B* **85**, 174533 (2012).
- [82] G. C. Ménard, F. K. Malinowski, D. Puglia, D. I. Pikulin, T. Karzig, B. Bauer, P. Krogstrup, and C. M. Marcus, Suppressing quasiparticle poisoning with a voltage-controlled filter, *Phys. Rev. B* **100**, 165307 (2019).